HYDROLOGY

More flow upstream and less flow downstream: The changing form and function of global rivers

Dongmei Feng[1]* and Colin J. Gleason[2]

We mapped daily streamflow from 1984 to 2018 in approximately 2.9 million rivers to assess recent changes to global river systems. We found that river outlets were dominated by significant decreases in flow, whereas headwaters were 1.7 times more likely to have significantly increased flow than decreased. These changes result in a significant upstream shift in streamflow experienced by about 29% of the global land surface. We found the most changes in the smallest steams in our study: increases in erosion potential (approximately 5% increase in stream power), flood frequency (approximately 42% increase in 100-year floods), and likely nutrient dynamics (altered seasonal flow regimes). We revealed these changes using "detail at scale" by mapping millions of individual rivers. Widely adopting this approach could reveal other changes to the hydrosphere.

Rivers are dendritic and hierarchically organized systems (*1*). Flowing from headwater to mouth, rivers regulate the transport and processing of water, energy, sediment, and nutrients, all of which affect humans and ecosystems. Along the course of a river, the continuous gradient of physical and hydrological conditions (often called the river "regime," e.g., flow, slope, and sediment particulate size) creates a variety of environments that provide different socioeconomic functions and support ecological communities (*2*). For example, headwaters are typically steep and fast-flowing streams carrying relatively coarse particulate matter (*3*). As rivers move downstream, their channels become wider and flatter and particulate matter is typically finer compared with their upstream counterparts (*4*). In response to these distinct hydrogeophysical and biochemical conditions, different dominant ecological communities form in rivers of different longitudinal locations, for example, invertivorous species in headwater streams, piscivorous and insectivorous species in mid-sized reaches, and planktivorous species in downstream waters (*2*). Rivers of different sizes also provide different socioeconomic services, e.g., recreational functions and community water needs from small rivers and energy, transportation, and irrigation supply from medium and large rivers. Therefore, the diverse ecological and socioeconomic services that a river system can offer at any one place is the integrated teamwork of all rivers before and after it, from headwater to river mouth, and sometimes over thousands of kilometers. A full understanding of river systems and their service capacity requires a global account of the physical conditions of all rivers, not just those that are easy to measure for geographical or political reasons.

River flow rate (also known as streamflow or discharge), defined as the water volume passing through the cross-section of a channel in a given time period with a unit of length^{3}time^{-1} (e.g., cubic meters per second), is one of the most important measurements of a river. Flow rate reflects a river's carrying capacity and regulates the exchange of nutrients, carbon, and energy, thereby controlling the functionality of a river system (*5*, *6*). The distribution of river flow across a river system largely defines hydrological and ecological heterogeneity. Any shift in flow distribution across or along its hierarchical network may cause the overall continuum response to be shifted, ultimately affecting the ecological and socioeconomic functionality of the entire river system (*2*). We have established the necessity of understanding rivers as connected systems from source to sea, but current knowledge of global river flow, especially recent spatiotemporal changes, does not capture this continuum. Therefore, although we generally understand the total flux of water and its recent changes from the land surface to the global ocean (*7*), we do not yet know the spatiotemporal patterns and gradients that comprise this bulk number and are essential for human society and ecosystems (*8*). In this study, we integrated primary satellite data and hydrologic models to comprehensively investigate the spatiotemporal distribution of daily river flow for ~2.9 million river reaches from 1984 to 2018 by creating the Global River Discharge Reanalysis (GRDR) dataset (*9*) (see the supplementary materials for details about how the GRDR was generated and for an evaluation of its efficacy). With this new global river product, we have quantified river flow and its recent temporal change across the full spatial distribution of nearly all mapped rivers globally.

To contextualize global streamflow relative to the continuum from sea to source, a standard device designed to understand rivers by their position in that continuum is needed. We used the classic Strahler stream order (SO) system for this purpose (*10*). SO assigns a numerical order to all streams, starting from 1 for headwaters and hierarchically increasing downstream with each tributary junction. Theory suggests that the number of streams, sub-basin areas, and flow all scale geometrically by SO within a basin (*11*, *12*). Organizing by SO introduces some challenges, including that "headwater" [SO = 1 (SO1)] in a global river network has in actuality numerous streams above it defined by the scale at which the network was made (*13*), and rivers of the same SO are not directly comparable across basins with different total orders. However, SO elegantly defines longitudinal relationships in basins as an underused device badly needed in global hydrology, and we used it here to reveal and contextualize changes in global rivers.

Results

We found that, on average, global rivers exported 101.96 km^3 of water into the ocean per day during the study period, but annual mean streamflow increased in headwater reaches and decreased in downstream sections globally, with substantial regional variations (Fig. 1). In the most upstream rivers (SO1) over all global basins, 17.1% showed significant increases in mean streamflow, whereas 9.9% showed significant decreases (Fig. 1A). By contrast, in the most downstream river reaches (SO ≥ 8), the significant increasing and decreasing changes were 11.9 and 44.2%, respectively (Fig. 1H). Aggregated globally, the annual flow in SO1 rivers showed a significant increase (Fig. 1A, inset plot), mainly due to increases occurring from December to May (fig. S5), whereas total flows in SO6 and SO ≥ 8 rivers showed significant decreases (Fig. 1, F and H, inset plots) that were less seasonally dependent (fig. S5). In general, the changes in flow shifted from significant increases to significant decreases when moving from headwaters to the outlets, with generally higher decrease rates in more downstream rivers, although some changes were insignificant (e.g., SO2 to SO5).

The maps in Fig. 1 were rendered from millions of individual river reaches, although that level of detail is not visible at this mapping scale. Changes in river streamflow showed substantial regional differences (Fig. 1). For example, for rivers of SO1 to SO3, central Africa, Europe, central Asia, western US, and southern South America were dominated by decreases in streamflow, whereas high mountain Asia (HMA), western and southern Africa, and the Arctic were hotspots of increasing trends, consistent with previous studies (*14*–*18*). Both increases and decreases were found in all regions mentioned above, but we highlight only the dominant signals due to the mapping scale

[1]Department of Chemical and Environmental Engineering, University of Cincinnati, Cincinnati, OH, USA. [2]Department of Civil and Environmental Engineering, University of Massachusetts, Amherst, MA, USA.
*Corresponding author. Email: fengdi@ucmail.uc.edu

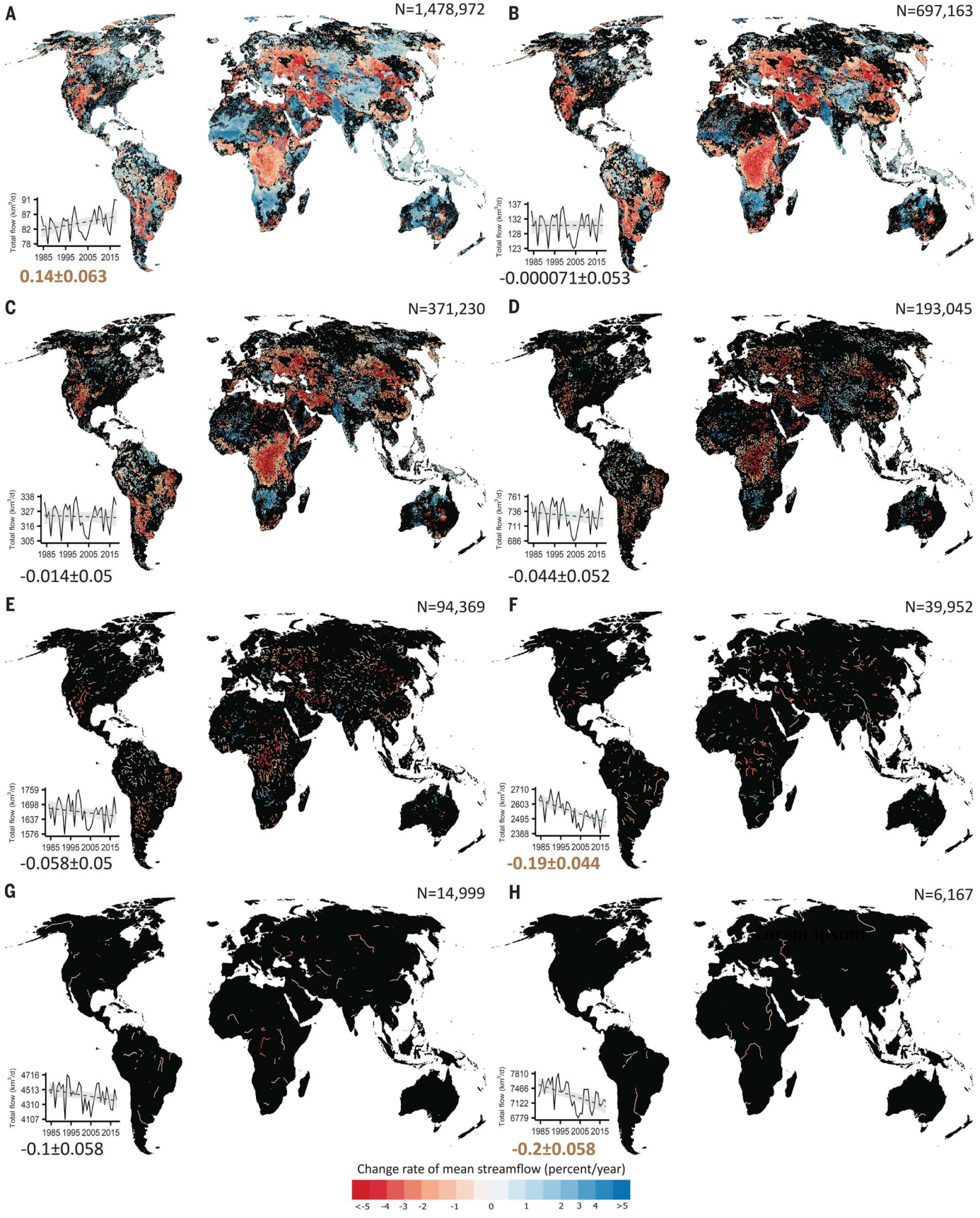

Fig. 1. Dominant changes in annual mean streamflow shift from increase to decrease as rivers go from headwaters to the mouth. (**A** to **H**) Maps showing the temporal change rate (%/year) of annual mean streamflow in river reaches with SO of 1, 2, 3, 4, 5, 6, 7, and ≥8, respectively, during 1984 to 2018. Lines

in red (blue) shades indicate significant ($P < 0.05$) decreasing (increasing) trends. Only significant changes are shown in the maps. Inset plots show the temporal changes in the total river flow carried by rivers of each SO. Solid black line is the time series, and the green dashed line is the fitted trend line at a 95% confidence interval (gray shading). The numbers under the inset plots are the change rate (%/year ± SE) of the total flow carried by a given SO, with bold brown indicating significant trends ($P < 0.05$) and black indicating insignificant trends ($P \geq 0.05$). The numbers in the top right of each subplot indicate the total number of reaches quantified for each SO.

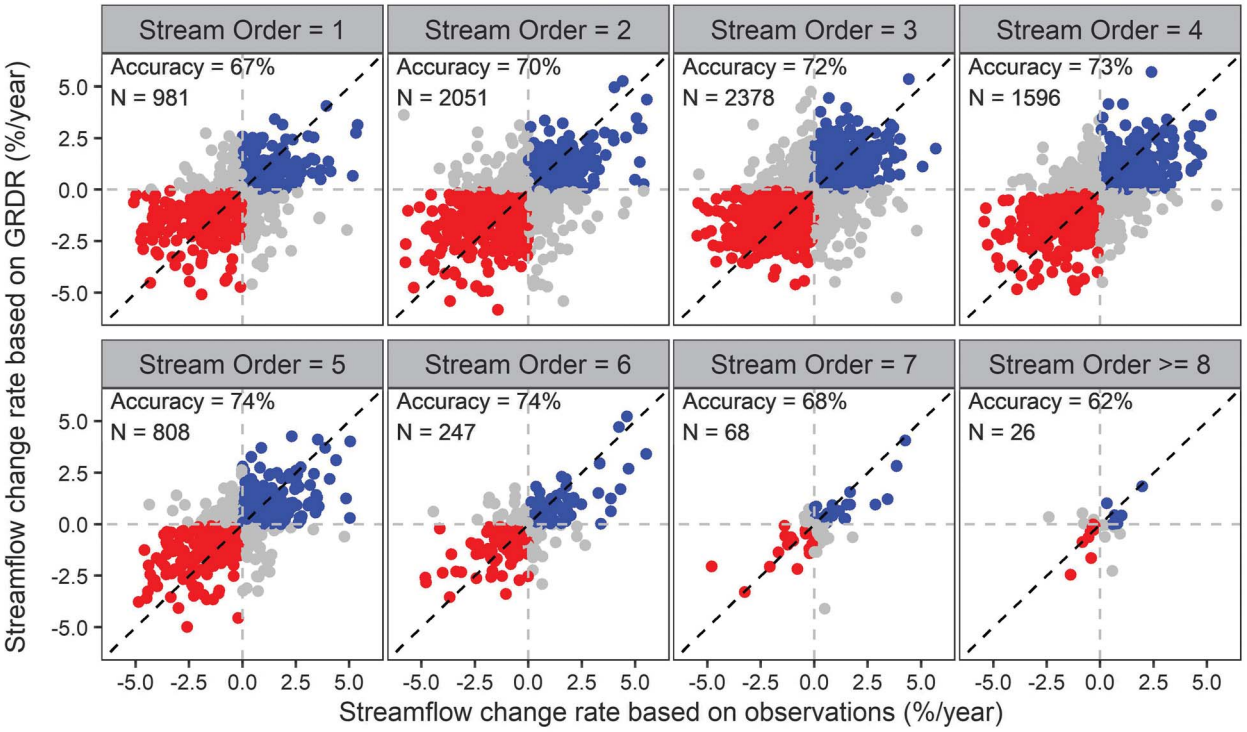

Fig. 2. Validating streamflow trend signals from GRDR using in situ daily observations from 8155 ground-based gauges. Blue (red) dots are increasing (decreasing) trends in streamflow for which GRDR agrees with gauge observations; gray dots are trends for which GRDR does not agree with gauge observations. The accuracy, defined as the rate of agreement with the directionality of trends (increase or decrease) in flow between GRDR and gauges, and the number of gauges evaluated (*N*) are indicated in the plot for each SO. All trends regardless of significance levels are shown in this figure, and the overall accuracy is 71.3%. The overall accuracy for only significant trends is 84.5% (results are shown in fig. S4).

limit. We also acknowledge that our results may not accurately capture the signals of some highly regulated rivers (e.g., the Colorado River), although GRDR improves streamflow simulation in regulated rivers (fig. S1).

We confirmed that GRDR's results are also evident in global in situ gauges, lending confidence to our findings. We compared change rates in streamflow between GRDR and gauge observations at 8155 gauges with at least 20 years of gauge data to ensure the reliability of trend signals (Fig. 2). We found that GRDR and gauges agreed with directionality of trends (increase or decrease) in flow for 71.3% of these gauges (Fig. 2), and for the 1777 gauges with significant trends in flow, the agreement was 84.5% (fig. S4). The gauge record does not contain enough samples to confirm within-basin trends and globally aggregated signals as shown in Fig. 1, because only a small portion (0.3%) of global rivers were represented by gauges here. This lack of gauge representation is one of the motivations for GRDR.

To generalize these changes in absolute streamflow and to consider basins as individual systems rather than aggregate across basins as in Fig. 1, we created the longitudinal hydrologic distribution index (LHDI) as a relative metric of streamflow shifts. LHDI calculates the distance between the centroid of basin flow and the basin outlet in units of SOs (see details in the supplementary materials). An increase or decrease in LHDI suggests an upstream or downstream shift in river flow distribution, respectively. Although LHDI has an abstract physical meaning (e.g., how many SOs from the outlet is the balance point for total basin flow?), it allows us to precisely and consistently categorize the changes in streamflow that we found above and assess their differences in space and time. LHDI also crucially allows us to quantitatively compare changes between basins to assess differences in flows independently of the number of SOs in a particular basin. LHDI shows a dominant upstream shift in streamflow in GRDR across global river basins (Fig. 3, A and B), consistent with results from other global discharge products (fig. S9) and the cross-basin SO trends shown in Fig. 1. It also suggests that 29% of the global land surface has seen a significant upstream shift in flow (Fig. 3A). Comparing Figs. 1 and 3 shows that the dominant global basin signal is indeed "upstream" whether in absolute or relative flows. We have repeated these analyses using topological distance from outlet to ensure that the SO unit did not induce these results and arrived at the same conclusions, as reported in the supplementary materials (figs. S10 and S11 and table S1). The relative LHDI is subject to upstream shifts where upstream rivers might not have increased actual flows. Consider the Plata, mapped in Fig. 1 as having dominant decreases in streamflow for SO1 to SO3. However, Fig. 3 shows the Plata as strongly shifting upstream in LHDI. In cases such as this, the dominant basin signal is a loss in downstream flow, which shifts the LHDI upstream without lower-order streams increasing flows.

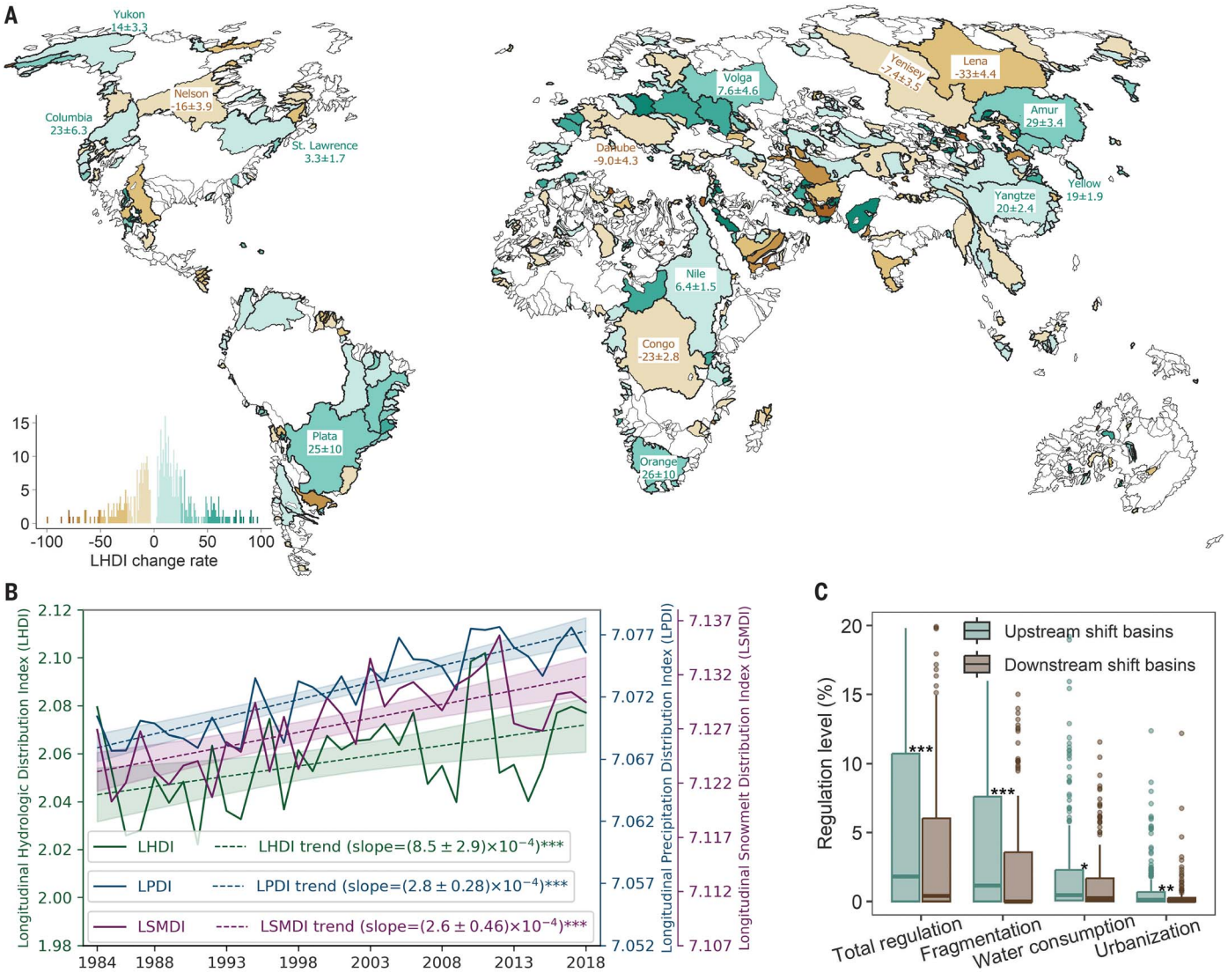

Fig. 3. Changes in the LHDI consistent with climate variations and human regulation levels. (**A**) LHDI change rates (×10^{-4} SO/year) in basins with the outlet SO ≥ 5 (in total 1384 basins) during 1984 to 2018. Only basins with significant changes ($P < 0.05$) are shown in color in the map. Large basins with significant changes in LHDI are denoted with the trend slopes (×10^{-4} SO/year ± SE). The histogram legend shows the distribution of significant changes in LHDI across all basins shown in the map. LHDI indicates how far the longitudinal center of a basin is from its outlet; an increase in LHDI (green shades in the map) therefore suggests an upstream shift whereas a decrease in LHDI (brown shades in the map) suggests a downstream shift. (**B**) Time series (solid line) and fitted trend lines (dashed line, trend slope ± SE, SO/year) at a 95% confidence interval (shading) of LHDI, LPDI, and LSMDI when all global rivers are aggregated. LPDI and LSMDI are similar to LHDI, but for precipitation and snowmelt, respectively. ***$P < 0.001$ for significant trends. The global upstream shift in discharge is concomitant with the significant upstream shifts in precipitation and snowmelt. (**C**) Comparison of regulation levels of different categories between upstream and downstream shift basins. ***$P < 0.001$, **$P < 0.01$, and *$P < 0.1$ for significant differences in mean regulation levels. In each boxplot, the top end of the whisker, the top and bottom of the box, and the thick solid line in the box are the maximum, 75th percentile, 25th percentile, and median regulation levels, respectively, excluding the outliers (dots). Only basins with significant changes in LHDI are considered. Upstream shift basins have more human regulation impacts than downstream shift basins. See the supplementary materials for the definitions of LHDI, LPDI, LSMDI, and regulations.

We found that global river flows are increasing in the headwaters while at the same time decreasing downstream, which is leading to an apparent upstream shift (Figs. 1 and 3B). This global upstream shift in the centroid of river streamflow is concomitant with upstream shifts in precipitation and snowmelt (Fig. 3B). Using a longitudinal precipitation distribution index (LPDI) and longitudinal snowmelt distribution index (LSMDI), we found that global LPDI and LSMDI have also been shifting upstream (Fig. 3B), mainly due to increases in precipitation and snowmelt in high-elevation rivers (fig. S12) and consistent with atmospheric warming (*15*, *19*). However, we did not find a significant correlation between the magnitudes of changes in LHDI and those of LPDI and LSMDI across basins, implying that upstream shifts are the result of interactions of multiple hydrologic components that vary in space and time.

We also found that basins with an upstream shift in streamflow have higher levels of human regulation than rivers with a downstream shift (Fig. 3C). The mean total regulation level is 8.3 and 5.0% for upstream and downstream shift basins, respectively, and similar patterns can be found for specific types of regulation such as

river fragmentation, water consumption, and urbanization (Fig. 3C). The total regulation level indicates an integrated impact of various human activities, and downstream rivers are generally more regulated (fig. S13). Going further, we queried databases of human water use covering our study period. However, such long-term human regulation data are difficult to create; only a few studies provide such products (*20*–*22*), and these are gridded at much larger areas than GRDR streams or tied to incomplete databases of global reservoirs. Nevertheless, it is important to contextualize shifts in flows with human water use. Using published water use data (*20*), we did not find significant relationships between water withdrawal changes and streamflow shifts (fig. S14 and table S2). Another recent study (*23*) did quantify global river storage and storage variability for our same basins and study period. As with water use, we did not find notable correlation with our results. Therefore, we argue that the streamflow shifts identified in our study are likely a combined result of climatic and anthropogenic impacts rather than being due to a single factor, as supported by the results shown in Fig. 3, B and C; figs. S12 to S14; and table S2. Nevertheless, the tendency of river systems to increase flows upstream and decrease them downstream is clear for relative and absolute flows in both the GRDR and the gauge record (Figs. 1 to 3).

Implications

These increases in flow in upstream rivers have important consequences for human and natural systems. River flow controls stream power, a measure of the ability of the stream to move sediment (particularly bedload; see the supplementary materials for the definition of stream power). Stream power varies directly with streamflow and therefore shows similar patterns of changes: Lower-order rivers increase stream power, whereas higher-order rivers decrease it (Fig. 4, A and B, and figs. S15 to S18). If the increased stream power in these upstream rivers occurs concurrently with increased transportable sediment supply, then cascading environmental and socioeconomic consequences are to be expected. A notable example is HMA, where accelerated glacial melt and permafrost destabilization, along with more frequent rain events, have significantly increased sediment supply to rivers (*15*, *24*–*26*). The increased stream power that we found in HMA upstream rivers (Fig. 1) combines with the increased sediment supply to substantially enhance riverine sediment transport (*15*, *27*), which results in reduced hydropower capacity due to trapping and/or siltation (*28*) and increased pollutant transport to the downstream freshwater ecosystem (*24*, *29*). In HMA, hydropower features prominently in the economic development of places such as Nepal, Bhutan, and Pakistan (*30*–*32*). These existing and/or planned hydropower facilities are placed in zones of most potential: the steepest mountain streams at low SO (*33*). Hydropower

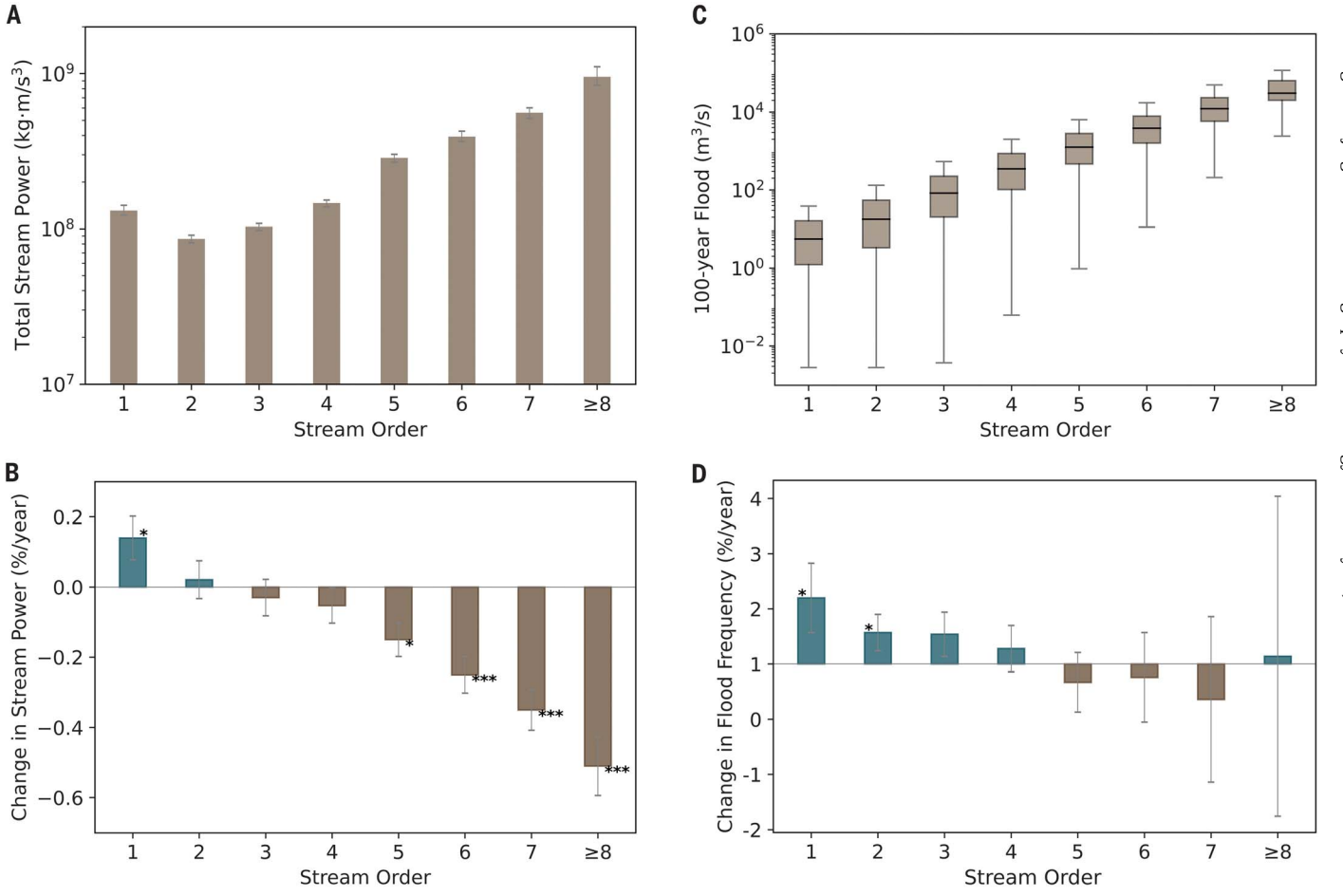

Fig. 4. Magnitudes and temporal changes of stream power and flood frequency vary substantially across SOs. (**A**) Total stream power produced by rivers of a given SO, with error bars indicating the annual variability during the study period. (**B**) Change rates of the total stream power for each SO during the study period, with green (brown) bars indicating increasing (decreasing) changes. (**C**) Magnitude distributions of 100-year floods of rivers across SOs. (**D**) Change rates of the frequency of 100-year floods during the study period. Error bars in (B) and (D) are 1 SE of the estimated change rates. ***$P < 0.001$ and *$P < 0.1$ in (B) and (D) for significant change rates. See the supplementary materials for the definitions of stream power, 100-year floods, and flood frequency.

turbines are highly sensitive to sediment, and mountain systems, particularly those in HMA, already require settling basins and siltation management to prevent accelerated wear on turbines (*28*, *34*). Increased stream power also indicates higher bank erosion potential, which could result in geomorphic changes. This increased bank erosion that we predict from GRDR is confirmed by widespread river widening in HMA revealed by long-term satellite data for the same period as this study (*18*).

Moreover, stream power controls the maximum size of particles that a river can move. The stream power generated by SO1 headwaters increased by 4.9% from the start to the end of the study period (Fig. 4B). Such increases may therefore have changed the sediment size distribution along riverine gradients by transporting larger particles farther downstream. Because headwater streams are hotspots for biogeochemical activities due to their close connection to hillslope and groundwater systems (*35*–*37*), changes in the erosion power in these watercourses may affect the entire river metabolism by altering the sources of sediment, carbon, and nutrients (*6*, *36*). In contrast to the upstream increase in stream power, downstream rivers have experienced significant decreases in the erosion potential (Fig. 4B). Previous studies reported that sediment export to the coast has been declining significantly due to sediment trapping behind dams, adversely affecting the development of deltas and associated ecosystems (*38*–*41*). The results from our study suggest that recent declines in sediment export due to trapping have been exacerbated by decreased stream power in middle to downstream rivers that slows bedload transport (Fig. 4B).

Our results also highlight another consequence of increased headwater flows for human and natural systems: flooding. We quantified the frequency of 100-year floods in rivers across orders and found that the occurrence of 100-year floods has increased by 42.0 and 20.0% during the study period for SO1 and SO2 rivers, respectively (Fig. 4D). By contrast, there were no significant changes in 100-year flood occurrence in downstream rivers (SO ≥ 3) (Fig. 4D). Previous studies have shown both increases and decreases in flood occurrence in rivers (*42*–*45*), although the warming climate enhances extreme precipitation events globally (*46*). Our study shows that changes in floods vary across the longitudinal locations, with the most upstream rivers experiencing the most significant changes (Fig. 4D). Although flood magnitudes in headwater streams are substantially lower than those in larger downstream rivers (Fig. 4C), the interaction with floodplains is more active and intense in headwaters compared with downstream. Therefore, increases in flood frequency in small rivers may have profound ecological and societal impacts given that they are more closely connected with natural riparian zones (*24*), and many human settlements are close to these rivers that often have less flood protection than more densely developed downstream settlements (*47*). More frequent flood pulses in upstream rivers mean a likely increased exchange of carbon and nutrients between river and floodplains and enhanced natural hydrologic connectivity to headwaters, which potentially affect ecological productivity (*48*–*51*). One prominent example is the Amazon headwaters, where increased streamflow has enhanced the spawning migration behavior of the goliath catfishes by providing improved hydrologic corridors to the spawning ground (*49*). This has important implications, not only for ecosystems, but also for local economies such as fisheries and food production (*49*). Similar analyses as in HMA and Amazon discussed above are possible in almost any other global region, although the context of GRDR's results depends both on the changes that GRDR reveals and the specific relationships among humans, ecosystems, and rivers in each location.

Beyond our findings of changes in streamflow patterns, flooding, and likely sediment transport, this study also represents a technical advance and a potential paradigm shift in studying global hydrology. Although GRDR is predominantly model driven, the billions of primary data points generated from satellites within GRDR show rivers as they are, not as idealized representations of themselves. Data assimilation allows near optimal use of these observations, together with global hydrologic models, to fuse daily meteorological data with intermittent satellite observations at scale. Our validation (figs. S1 to S3) proves that GRDR is more accurate than current global hydrologic modeling without satellite augmentation and allows us to clearly define the global riverine water cycle in sharp relief. GRDR provides essential data for enabling or updating the estimates of critical river variables such as carbon emission (*5*, *52*) and riverine carbon flux (*53*) and could therefore improve our understanding of global river processes (*6*). As riverine satellite data proliferate—for example, the Surface Water and Ocean Topography (SWOT) mission was purpose-built for monitoring global rivers and now is in orbit (*54*)—we expect many more studies like ours to reveal further changes to the hydrosphere and their consequences for humans and ecosystems that are an accurate expression of individualized river hydraulics and hydrology at global scales. The "detail at scale" that we have shown here bridges longstanding divides between primary measurement and modeling in hydrology and is only possible with modern remote sensing and computational resources. Future studies should use this framing, in which global hydrology is cast as a collection of millions of individual rivers, to further our understanding of all global rivers. Doing so will reveal changes in the form and function of our global hydrosphere beyond those that we have identified here.

REFERENCES AND NOTES

1. C. E. Torgersen *et al.*, *Biol. Rev. Camb. Philos. Soc.* **97**, 481–504 (2022).
2. R. L. Vannote, G. W. Minshall, K. W. Cummins, J. R. Sedell, C. E. Cushing, *Can. J. Fish. Aquat. Sci.* **37**, 130–137 (1980).
3. K. L. Halwas, M. Church, *Geomorphology* **43**, 243–256 (2002).
4. L. C. Smith, *Rivers of Power: How a Natural Force Raised Kingdoms, Destroyed Civilizations, and Shapes Our World* (Penguin Books, 2020).
5. S. Liu *et al.*, *Proc. Natl. Acad. Sci. U.S.A.* **119**, e2106322119 (2022).
6. T. J. Battin *et al.*, *Nature* **613**, 449–459 (2023).
7. L. Su *et al.*, *J. Hydrol. (Amst.)* **563**, 818–833 (2018).
8. J. A. Downing *et al.*, *Inland Waters* **2**, 229–236 (2012).
9. D. Feng, C. J. Gleason, Global River Discharge Reanalysis dataset (GRDR) (2024); https://zenodo.org/records/13951712.
10. A. N. Strahler, *Eos* **38**, 913–920 (1957).
11. R. E. Horton, *Geol. Soc. Am. Bull.* **56**, 275–370 (1945).
12. J. W. Kirchner, *Geology* **21**, 591–594 (1993).
13. G. Amatulli *et al.*, *Earth Syst. Sci. Data* **14**, 4525–4550 (2022).
14. S. Karam, O. Seidou, N. Nagabhatla, D. Perera, R. M. Tshimanga, *Clim. Change* **170**, 40 (2022).
15. D. Li *et al.*, *Science* **374**, 599–603 (2021).
16. D. Feng *et al.*, *Nat. Commun.* **12**, 6917 (2021).
17. J. C. Hammond *et al.*, *Water Resour. Res.* **58**, e2022WR031930 (2022).
18. D. Feng, C. J. Gleason, X. Yang, G. H. Allen, T. M. Pavelsky, *Water Resour. Res.* **58**, WR031712 (2022).
19. R. R. Cordero *et al.*, *Sci. Rep.* **9**, 16945 (2019).
20. Z. Huang *et al.*, *Hydrol. Earth Syst. Sci.* **22**, 2117–2133 (2018).
21. Y. Wada, D. Wisser, M. F. P. Bierkens, *Earth Syst. Dyn.* **5**, 15–40 (2014).
22. N. Hanasaki *et al.*, *Hydrol. Earth Syst. Sci.* **17**, 2375–2391 (2013).
23. E. L. Collins *et al.*, *Nat. Geosci.* **17**, 433–439 (2024).
24. T. Zhang *et al.*, *Sci. Adv.* **9**, eadi5019 (2023).
25. A. F. Lutz, W. W. Immerzeel, A. B. Shrestha, M. F. P. Bierkens, *Nat. Clim. Chang.* **4**, 587–592 (2014).
26. D. Treichler, A. Kääb, N. Salzmann, C.-Y. Xu, *Cryosphere* **13**, 2977–3005 (2019).
27. T. Zhang *et al.*, *Nat. Rev. Earth Environ.* **3**, 832–851 (2022).
28. D. Li *et al.*, *Nat. Geosci.* **15**, 520–530 (2022).
29. M. Liu *et al.*, *Nat. Geosci.* **14**, 672–677 (2021).
30. A. Hussain *et al.*, *Renew. Sustain. Energy Rev.* **107**, 446–461 (2019).
31. F. Alam *et al.*, *Energy Procedia* **110**, 581–585 (2017).
32. U. K. Mirza, N. Ahmad, T. Majeed, K. Harijan, *Renew. Sustain. Energy Rev.* **12**, 1641–1651 (2008).
33. D. Kumar, S. S. Katoch, *Renew. Energy* **77**, 571–578 (2015).
34. C. Hauer *et al.*, *Renew. Sustain. Energy Rev.* **98**, 40–55 (2018).
35. G. H. Allen *et al.*, *Nat. Commun.* **9**, 610 (2018).
36. T. Gomi, R. C. Sidle, J. S. Richardson, *Bioscience* **52**, 905–916 (2002).
37. K. E. Bencala, M. N. Gooseff, B. A. Kimball, *Water Resour. Res.* **47**, 2010WR010066 (2011).
38. E. N. Dethier, C. E. Renshaw, F. J. Magilligan, *Science* **376**, 1447–1452 (2022).
39. J. P. M. Syvitski *et al.*, *Nat. Geosci.* **2**, 681–686 (2009).
40. H. Gupta, S.-J. Kao, M. Dai, *J. Hydrol. (Amst.)* **464–465**, 447–458 (2012).
41. J. P. M. Syvitski, C. J. Vörösmarty, A. J. Kettner, P. Green, *Science* **308**, 376–380 (2005).
42. H. X. Do *et al.*, *Hydrol. Earth Syst. Sci.* **24**, 1543–1564 (2020).
43. G. Blöschl *et al.*, *Nature* **573**, 108–111 (2019).
44. I. Mallakpour, G. Villarini, *Nat. Clim. Chang.* **5**, 250–254 (2015).
45. L. Gudmundsson *et al.*, *Science* **371**, 1159–1162 (2021).
46. M. Rodell, B. Li, *Nat. Water* **1**, 241–248 (2023).
47. Y. Fang *et al.*, *Earths Futur.* **6**, 1134–1145 (2018).
48. A. J. King, Z. Tonkin, J. Mahoney, *River Res. Appl.* **25**, 1205–1218 (2009).
49. D. Feng *et al.*, *Hydrol. Processes* **34**, 5402–5416 (2020).
50. R. B. Barthem *et al.*, *Sci. Rep.* **7**, 41784 (2017).
51. G. Baumgartner, K. Nakatani, L. C. Gomes, A. Bialetzki, P. V. Sanches, *Environ. Biol. Fishes* **71**, 115–125 (2004).
52. G. H. Allen, T. M. Pavelsky, *Science* **361**, 585–588 (2018).
53. M. Li *et al.*, *Ecol. Indic.* **80**, 40–51 (2017).

54. S. Biancamaria, D. P. Lettenmaier, T. M. Pavelsky, *Surv. Geophys.* **37**, 307–337 (2016).

ACKNOWLEDGMENTS

We acknowledge and thank all mentioned data and method developers for producing the data and code and making them publicly available. We also thank P. Bates, J. Fayne, and T. Pavelsky for providing helpful suggestions and thank P. Devkota, P. Ramtel, A. Regmi, and S. Mahato for assistance with data collection and visualization. **Funding:** This work was supported by the NASA Terrestrial Hydrology Program (grant 80NSSC22K0987 to D.F. and C.J.G.); the NASA Early Career Investigator Program (grant 80NSSC24K1048 to D.F.); the NASA Surface Water and Ocean Topography (SWOT) Program (grant 80NSSC24K1654 to D.F. and grant 80NSSC20K1141 to C.J.G.); and the NASA New Investigator Program (grant 80NSSC18K0741 to C.J.G.). **Data availability:** GLOW is publicly available at https://doi.org/10.5281/zenodo.6425657. GRFR products were previously published and publicly available at https://www.reachhydro.org/home/records/grfr. GloFAS products were previously published and publicly available at https://ewds.climate.copernicus.eu/datasets/cems-glofas-historical?tab=overview. ERA5 Climate data are available at https://cds.climate.copernicus.eu/datasets. MERIT DEM is available at http://hydro.iis.u-tokyo.ac.jp/~yamadai/MERIT_DEM/. MERIT-Basin hydrography is available at https://www.reachhydro.org/home/params/merit-basins. GROD is available at https://zenodo.org/record/5793918. GOODD is available at http://www.globaldamwatch.org. The river regulation data are available at https://doi.org/10.6084/m9.figshare.7688801. RiverATLAS data are available at https://www.hydrosheds.org/hydroatlas. Global monthly water withdrawal data are available at https://doi.org/10.5281/zenodo.897933. In situ river discharge data were collected from the US Geological Survey (https://waterdata.usgs.gov/nwis/sw), Environment and Climate Change Canada (https://www.canada.ca/en/environment-climate-change.html), Centre d'Expertise Hydrique du Québec (https://www.cehq.gouv.qc.ca/), Global Runoff Dataset Center (https://www.bafg.de/GRDC/EN/04_spcldtbss/42_EWA/ewa_node.html), R-ArcticNET (https://www.r-arcticnet.sr.unh.edu/v4.0/index.html), Arctic Great River Observatory (https://arcticgreatrivers.org/), China Hydrology Data Project (https://www2.oberlin.edu/faculty/aschmidt/chdp/index.html, the data was directly from the author of the project), India Water Resources Information System (https://www.indiawris.gov.in/wris/#/DataDownload), Brazil National Water Agency (https://www.snirh.gov.br/hidroweb/apresentacao), Spain Digital hydrological yearbook (https://ceh.cedex.es/anuarioaforos/GALICIA%20COSTA_csv.asp), Thailand Royal Irrigation Department (http://hydro.iis.u-tokyo.ac.jp/GAME-T/GAIN-T/routine/rid-river/index.html), Chile Center for Climate and Resilient Research (https://www.cr2.cl/download/cr2_qflxdaily_2018-zip/), Australia Bureau of Meteorology (http://www.bom.gov.au/). The river network underlying GRDR is available at https://drive.google.com/drive/folders/1uCQFmdxFbjwoT9OYJxw-pXaP8q_GYH1a. GRDR is available at https://zenodo.org/records/13951712. **Code availability:** The geoBAMr package is available at https://github.com/craigbrinkerhoff/geoBAMr. The data assimilation code is available at https://github.com/Fluvial-UMass/SIRD_Missouri. The code used for generating the figures in this study is available at https://github.com/dongmeifeng-2019/GRDR. **Author contributions:** Conceptualization: D.F., C.J.G.; Funding acquisition: D.F., C.J.G.; Investigation: D.F., C.J.G.; Methodology: D.F., C.J.G.; Visualization: D.F.; Writing – original draft: D.F.; Writing – review & editing: D.F., C.J.G. **Competing interests:** The authors declare no competing interests.

SUPPLEMENTARY MATERIALS

science.org/doi/10.1126/science.adl5728
Materials and Methods
Supplementary Text
Figs. S1 to S19
Tables S1 to S2
References (*55*–*81*)

Submitted 30 October 2023; accepted 16 October 2024
10.1126/science.adl5728